

## Identification of $p$ -wave superconductors

L. J. Buchholtz\*

*Institut für Festkörperforschung der Kernforschungsanlage, Jülich, 5170 Jülich,  
Federal Republic of Germany*

G. Zwirgagl

*Max-Planck-Institut für Festkörperforschung, 7000 Stuttgart 80,  
Federal Republic of Germany*

(Received 28 January 1981)

Tunneling spectra of hypothetical  $p$ -wave and conventional  $s$ -wave superconductors are expected to differ significantly. There is a bulk effect which arises due to the differences in the structure of the Cooper pairs, and a surface effect, which dominates, and is associated with the interface of the tunnel junction. We calculate the tunneling density of states of a  $p$ -wave superconductor in a magnetic field and discuss particular features which allow experimental identification of  $p$ -wave superconductors.

### I. INTRODUCTION

Experimental progress in superconductor research over the last few years has rekindled theoretical speculation as to the possible existence of  $p$ -wave superconductors. In particular, the progressive technical mastery of difficult tunnel-junction experiments by Merservey and his co-workers<sup>1</sup> has prompted them to propose those methods as a likely means of identifying and labeling triplet pairing, and of distinguishing it from the more common singlet pairing.

Following up this train of thought we would like to present here a qualitative discussion of  $p$ -wave paired Fermi systems emphasizing properties which would allow an experimental discrimination between the two forms of pairing. The features chosen for discussion were response to magnetic fields, response to impurities, and behavior in the presence of a reflecting surface (surface pairbreaking). It seemed apparent that any of the experiments under consideration would involve all three attributes (in perhaps undetermined measure). A cogent interpretation of the results would then presuppose a certain familiarity with these effects, singly and combined, and our interest here is to pursue that acquaintanceship further. The technical tools we employ are commonly recognized under the nomenclature "quasiclassical methods."<sup>2</sup> We expect no significant strong-coupling effects and apply these methods in the form correct to the accuracy of normal weak-coupling theory. Approximations enter only through the introduction of individual models for each of the properties investigated.

We begin the discussion with a brief exposition of the quasiclassical techniques used emphasizing the general structures involved. The individual cases are then presented, and we delineate details of the models used and results obtained.

### II. THEORETICAL BACKGROUND

The characteristic scales of energy and length in superconducting phenomena are set by  $k_B T_c$  and  $\xi_0 = \hbar v_F / \pi k_B T_c$ . The quasiclassical formulation of superconductivity proceeds by restricting one's attention exclusively to variations along these scales. This is effected by explicit elimination from the theory, at the very outset, of properties determined by the Fermi wavelength  $k_F^{-1} \ll \xi_0$ , and the Fermi energy  $E_F \gg k_B T_c$ . The advantage gained is a very considerable simplification, elegance, and calculational ease. An important aspect of the spirit involved is that, since the traditional BCS approach is restricted in accuracy by the quantity  $k_B T_c / E_F$  anyway, one has made progress by fully acknowledging this fact and eliminating as many intermediate steps as possible. One might add that the quasiclassical formulation lends itself to immediate generalization encompassing "strong-coupling" phenomena as well. However, we anticipate no significant strong-coupling corrections to the properties discussed in this paper and shall not pursue this feature further here.

We next briefly introduce the general mathematical framework employed in these calculations, relying on Ref. 2 for the detailed derivations, discussions, and notations. The underlying structure proceeds from formal many-body perturbation theory expressed in terms of the thermodynamic (imaginary-time) Green's functions. We use the  $4 \times 4$  matrix notation which contains the "anomalous" Green's functions in the off-diagonal quadrants.

In what follows only the static limit will be important, and consequently only one frequency, the energy variable, will appear as an argument. The basic working tool is the "quasiclassical" or " $\xi$ -integrated" Green's function  $\hat{g}(\vec{k}; \vec{R}; \epsilon_n)$ . Loosely speaking,  $\hat{g}$  has

been derived from the full one-particle Green's function by integrating over the magnitude of the relative spatial variable's Fourier components. As written,  $\bar{\mathbf{R}}$  is the center of mass spatial coordinate,  $\hat{k}$  is the remaining direction of the Fourier-transformed relative spatial coordinate,  $\epsilon_n$  is the Fourier-transformed relative time coordinate at the Matsubara frequencies, and the caret denotes the  $4 \times 4$  matrix notation. The importance of quasiclassical Green's functions stems, first, from the fact that the theory may be cast exclusively in terms of them, and second, that the expectation value of all interesting observables may be expressed through them as follows:

$$\langle A(\bar{\mathbf{R}}) \rangle = T \sum_n N(E_F) \int \frac{d^2 \hat{k}}{4\pi} \frac{1}{2} \text{Tr}_4[\hat{a}_{qp}(\hat{k}) \hat{g}(\hat{k}; \bar{\mathbf{R}}; \epsilon_n)] , \quad (2.1)$$

where  $a_{qp}$  is, in the notation of Ref. 3, the quasiparticle operator corresponding to the variable  $A(\bar{\mathbf{R}})$ . The equations determining  $\hat{g}$  are derived in turn from the Dyson equation determining the full Green's function. They take the form of a transportlike equation plus a normalization condition. In the static limit they are

$$i\epsilon_n(\hat{\tau}_3 \hat{g}(\hat{k}; \bar{\mathbf{R}}; \epsilon_n)) + i v_F \hat{k} \cdot \nabla_{\bar{\mathbf{R}}} \hat{g}(\hat{k}; \bar{\mathbf{R}}; \epsilon_n) - \hat{\tau}_3 \hat{\sigma}(\hat{k}; \bar{\mathbf{R}}; \epsilon_n) \times \hat{g}(\hat{k}; \bar{\mathbf{R}}; \epsilon_n) + \hat{g}(\hat{k}; \bar{\mathbf{R}}; \epsilon_n) \hat{\sigma}(\hat{k}; \bar{\mathbf{R}}; \epsilon_n) \hat{\tau}_3 = 0 , \quad (2.2a)$$

and

$$\tau_3 \hat{g}(\hat{k}; \bar{\mathbf{R}}; \epsilon_n) \hat{\tau}_3 \hat{g}(\hat{k}; \bar{\mathbf{R}}; \epsilon_n) = -\pi^2 \hat{1} , \quad (2.2b)$$

where  $\hat{\sigma}$  is the quasiparticle self-energy. Closing the circle of equations requires defining  $\hat{\sigma}$  as a functional of  $\hat{g}$ . This is denoted the "self-energy equation" and will provide the order parameter "gap equation."

The only remaining specification required is the boundary condition at a reflecting surface, which we excerpt from Ref. 2 as

$$\Delta \hat{g}(\hat{k}; \hat{\mathbf{R}}_{\text{surf}}; \epsilon_n) \hat{\tau}_3 \Delta \hat{g}(\hat{k}; \hat{\mathbf{R}}_{\text{surf}}; \epsilon_n) = 0 , \quad (2.3)$$

with

$$\Delta \hat{g} = -\frac{i}{v_F \hat{k} \cdot \hat{n}} (\hat{\tau}_3 \hat{t} \hat{g} - \hat{g} \hat{t} \hat{\tau}_3) , \quad (2.4)$$

where  $\hat{t}$  is the surface  $t$  matrix. Equations (2.2)–(2.4) serve then as the basis for all the calculations discussed here.

### III. MAGNETIC AND IMPURITY RESPONSE

In the following section we discuss the density of states of a bulk system with a magnetic field, coupled only to the electronic spins. We ignore, for simplic-

ity, all orbital effects of a magnetic field. The hypothetical triplet superconductor will be characterized by an order parameter of the BW type. This choice suggests itself by the fact that, within the weak-coupling theory and within the Eliashberg theory of superconductivity, this is the most stable *p*-wave state. Due to the symmetry of the order parameter all spin-independent properties, in particular the excitation spectrum of the pure bulk system, are exactly the same as those of an ordinary BCS superconductor.

A magnetic field acting on the spins, however, shifts the excitation energies of the single-particle states  $k \uparrow, -k \downarrow$ :

$$\epsilon_{k \downarrow} = \epsilon_k - \frac{1}{2} \mu_{\text{eff}} H , \quad \epsilon_{k \uparrow} = \epsilon_k + \frac{1}{2} \mu_{\text{eff}} H ,$$

where the effective moment  $\mu_{\text{eff}}$  accounts for the Stoner enhancement as well as for the electron-phonon mass renormalization. The equal spin-pairing states,  $|\uparrow\uparrow\rangle$  and  $|\downarrow\downarrow\rangle$ , are not affected by this shift and the corresponding excitation spectrum remains unchanged exhibiting a single peak at the original gap edge [Fig. 1(a)]. [Since we restrict ourselves to low magnetic fields, we can neglect the deformation of the order parameter which is of order  $(\mu_{\text{eff}} H / \Delta)^2$ .]

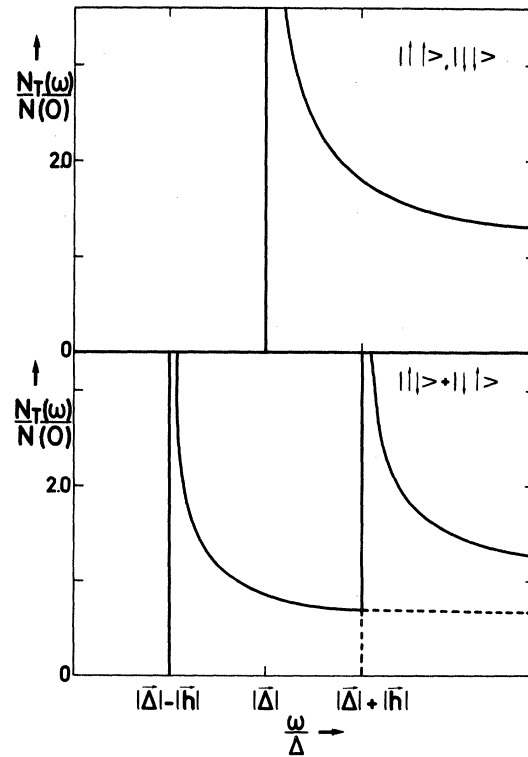


FIG. 1. Excitation spectra for equal-spin pairs and opposite-spin pairs in the presence of a magnetic field.

A pure opposite spin-pairing state,  $(1/\sqrt{2})(|\uparrow\downarrow\rangle - |\downarrow\uparrow\rangle)$ , on the other hand, behaves exactly like a singlet state as can be seen from Fig. 1(b). We observe pair breaking which is reflected in a Zeeman-split spectrum.

In the case of a general triplet state the spectrum exhibits more complicated features which can be calculated easily from the transportlike equations,

$$\begin{aligned} i\epsilon_n(\hat{\tau}_3\hat{g}_0) - \hat{\tau}_3\hat{\sigma}\hat{g}_0 + \hat{g}_0\hat{\sigma}\hat{\tau}_3 &= 0, \\ \tau_3\hat{g}\hat{\tau}_3\hat{g} &= -\pi^2\hat{1}, \end{aligned} \quad (3.1)$$

where we included the Zeeman contribution

$$\frac{1}{2}\mu_{\text{eff}}\vec{H}_{\text{ext}} \cdot \vec{\sigma} = \vec{h} \cdot \vec{\sigma}$$

$$\begin{aligned} g_s(\hat{k}; \epsilon_n) &= -\frac{\pi}{2} i\epsilon_n \frac{d(\hat{k}) + [d^2(\hat{k}) - \eta^2(\hat{k})]^{1/2}}{[d^2(\hat{k}) - \eta^2(\hat{k})]^{1/2} \left( \frac{1}{2} [d(\hat{k}) + [d^2(\hat{k}) - \eta^2(\hat{k})]^{1/2}] |\vec{h}|^2 \right)^{1/2}}, \\ \vec{g}_v(\hat{k}; \epsilon_n) &= \frac{x(\hat{k})g_s(\hat{k}; \epsilon_n)}{i\epsilon_n} [x(\hat{k})\vec{h} - \vec{\Delta}(\hat{k})]. \end{aligned} \quad (3.4)$$

For real frequencies  $\omega$  and fixed direction  $\hat{k}$  the excitation spectrum,  $-(1/\pi)\text{Im}g_s$ , may exhibit one, two, or three peaks depending on the relative orientation of the magnetic field and the order-parameter vector. Secondly, if the direction of the order-parameter vector varies over the Fermi surface the quasiparticle states will not be in general eigenstates of a spin projection.

The properties which distinguish the pure bulk triplet superconductor from the ordinary singlet-paired one are also reflected in the total density of states and the polarization which is shown in Fig. 2. The total density of states should be compared with Fig. 1(b) since, as mentioned above, the corresponding *s*-wave curve is identical to the one obtained for pure opposite spin pairing.

In the triplet case the excitation spectrum has a square-root dependence starting at the energy  $\omega = |\vec{\Delta}| - |\vec{h}|$ . At the original gap edge we observe a logarithmic singularity originating from excitations from equal spin pairs. The second branch of the quasiparticle spectrum begins at a frequency  $\omega = (\Delta^2 + h^2)^{1/2}$ , leads to a maximum at  $\omega = |\vec{\Delta}| + |\vec{h}|$ , and decreases for higher frequencies.

For the triplet superconductor the polarization,

$$P(\omega) = \frac{N_1(\omega) - N_1(\omega)}{N_1(\omega) + N_1(\omega)} \quad (3.5)$$

is a continuous function of the excitation energy  $\omega$ ; in addition, its absolute value is lower than in its (ideal) singlet-paired counterpart where the polarization is equal to 1 for the lower quasiparticle branch

in the self-energy

$$\hat{\sigma} = \begin{pmatrix} \vec{h} \cdot \vec{\sigma} & (-\vec{\Delta} \cdot \vec{\sigma}) i\sigma_2 \\ i\sigma_2 \vec{\Delta} \cdot \vec{\sigma} & (\sigma_2 \vec{h} \cdot \vec{\sigma}) \sigma_2 \end{pmatrix}. \quad (3.2)$$

We solve for the normal part  $g_s + \vec{g}_v \cdot \vec{\sigma}$  of the Green's function  $\hat{g}_0$ . Introducing the abbreviations

$$\begin{aligned} \eta(\hat{k}) &= 2|\vec{\Delta}(\hat{k}) \cdot \vec{h}|, \\ d(\hat{k}) &= \epsilon_n^2 + |\vec{\Delta}(\hat{k})|^2 + |\vec{h}|^2, \end{aligned} \quad (3.3)$$

$$x(\hat{k}) = \frac{1}{\eta(\hat{k})} \{d(\hat{k}) - [d^2(\hat{k}) - \eta^2(\hat{k})]^{1/2}\},$$

we obtain

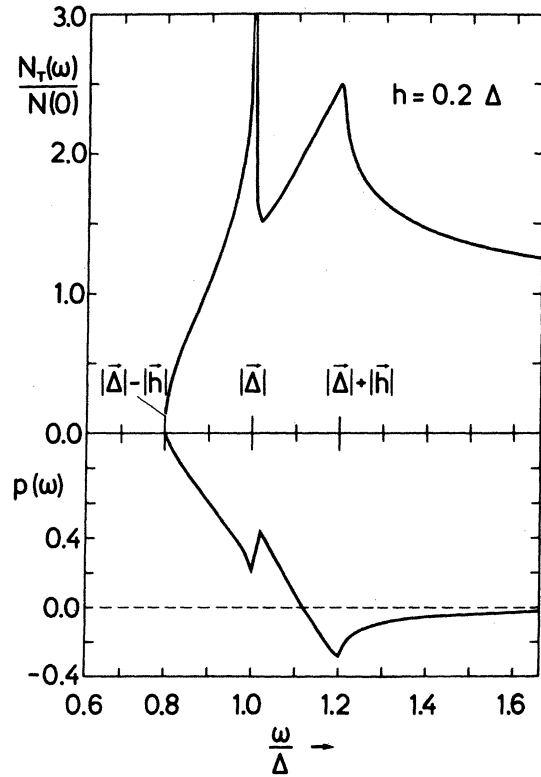


FIG. 2. Total density of states,  $N_T(\omega)/N(0)$ , and polarization,  $p(\omega)$ , of an ideal bulk triplet superconductor in a magnetic field.

( $\Delta - h \leq \omega < \Delta + h$ ), which jumps to  $-1$  at  $\omega = \Delta + h$  and then decreases to zero. The reduction of polarization is due to the presence of equal spin-pairing states because the excitations contribute equally to  $N_{\uparrow}(\omega)$  and  $N_{\downarrow}(\omega)$ . As a consequence the polarization is reduced near the original gap edge  $\omega = |\bar{\Delta}|$ .

These results for the pure bulk case confirm Merservey's idea that one can distinguish singlet and triplet superconductors by the density of states and the polarization in a magnetic field.

In the presence of impurities the total density of states and the polarization of an *s*-wave superconductor remain the same provided that spin-orbit scattering can be neglected. This is a consequence of the fact that momentum scattering does not affect significantly this type of pairing. In an anisotropic superfluid, however, it establishes an important pair-breaking mechanism which tends to suppress superconductivity. This is in close analogy to spin scattering from magnetic impurities in a conventional *s*-wave superconductor and, in the absence of an external magnetic field we expect similar results in both cases.

Impurities establish strong perturbations  $v \sim E_F$  varying on the microscopic length scale  $1/k_F$ . They are accounted for by a scattering term which we evaluate within the self-consistent *t*-matrix approximation. We calculate the single impurity *t* matrix while we include the scattering from all other centers in an effective medium which is determined self-consistently. This procedure is correct to leading or-

ders in  $1/lk_F$  where  $l$  and  $k_F$  denote the electron mean free path and the Fermi wave vector. We note that this is *not* a perturbation expansion in powers of the impurity concentration since all orders of  $l/\xi_0$  are retained.

We proceed in the following way: first we calculate the *t* matrix of a single impurity which allows us to understand the very dilute limit and gives us some insight into the structure of the spectrum. In the second step we extend our calculations to finite impurity concentrations. We start from the conventional *t*-matrix equation

$$\hat{t} = \hat{v} + \hat{v} \hat{g}_0 \hat{t} \quad , \quad (3.6)$$

with

$$\hat{v} = v \hat{\tau}_3 \quad ,$$

$\hat{g}_0$  is the quasiclassical Green's function in the presence of a magnetic field.

In the following we restrict ourselves to the special case of pure *s*-wave scattering. The corresponding *t* matrix does not depend upon the direction  $\hat{k}$  on the Fermi surface and Eq. (3.6) becomes

$$t = v_s \hat{\tau}_3 + v_s \hat{\tau}_3 N(0) \int \frac{d^2 \hat{k}}{4\pi} \hat{g}_0(\hat{k}; \epsilon_n) \hat{t} \quad . \quad (3.7)$$

The anomalous parts of the matrix Green's function are odd in the variable  $\hat{k}$ ; therefore they do not contribute to the *t* matrix in the *s*-wave approximation. Equation (3.7) is inverted easily yielding

$$\hat{t} = t_0 \hat{\tau}_3 + t_0 \hat{\tau}_3 v_s N(0) \begin{pmatrix} \langle g_s^0 \rangle + \langle \bar{g}_v \rangle \cdot \bar{\sigma} & 0 \\ 0 & \langle g_s^0 \rangle + \sigma_2 \langle \bar{g}_v \rangle \cdot \bar{\sigma} \sigma_2 \end{pmatrix} \quad , \quad (3.8)$$

with

$$t_0 = v_s \frac{1 - [N(0)v_s]^2 (\langle g_s^0 \rangle - \langle \bar{g}_v \rangle \cdot \bar{\sigma})^2}{[1 - [N(0)v_s]^2 (\langle g_s^0 \rangle + |\langle \bar{g}_v \rangle|^2)] [1 - [N(0)v_s]^2 (\langle g_s^0 \rangle - |\langle g_v^0 \rangle|^2)]} \quad . \quad (3.9)$$

Here we introduced the following notations and abbreviations

$$\langle g_s^0 \rangle = \int \frac{d^2 \hat{k}}{4\pi} g_s^0(\hat{k}; \epsilon_n) \quad , \quad \langle \bar{g}_v \rangle = \int \frac{d^2 \hat{k}}{4\pi} \bar{g}_v^0(\hat{k}; \epsilon_n) \quad .$$

Since  $t_0 \hat{\tau}_3$  does not contribute to  $\hat{\tau}_3 \hat{\sigma} \hat{g}_0 - \hat{g}_0 \hat{\sigma} \hat{\tau}_3$  this term is ignored in the proceeding calculation. There is a close analogy between this single impurity *t* matrix and the one obtained for spin scattering from a classical spin in an ordinary singlet superconductor.<sup>4</sup> In the absence of a magnetic field, the *t* matrix (3.8) has two poles at

$$\omega_B = \pm [1 + [\pi N(0)v_s]^2]^{-1/2} \quad ,$$

corresponding to two bound states in the excitation

gap. This fact which is a direct consequence of the singularity of  $\hat{g}_0$  at the gap edge highlights the inadequacy of the Born approximation. In a weak magnetic field one observes a Zeeman splitting of these states.

For finite impurity concentrations these discrete bound states will form bands which spread out until the gaps disappear. For a more quantitative discussion we characterize our system by the reduced scattering cross section  $\bar{\sigma}$  and the quasiparticle lifetime  $\tau_s$  in the normal state. The reduced scattering cross section  $\bar{\sigma}$  is defined as the ratio of the normal-state total cross section  $\sigma_{\text{tot}}$  divided by the maximum value in the unitary limit

$$\sigma_{\text{max}} = \frac{4\pi}{k_F^2} \quad , \quad \bar{\sigma} = \frac{\sigma_{\text{tot}}}{\sigma_{\text{max}}} = \frac{[\pi N(0)v_s]^2}{1 + [\pi N(0)v_s]^2} \quad ;$$

it measures the strength of the single impurity potential. The single scatterer bound states in zero magnetic field are located at  $\omega_B = \pm(1 - \bar{\sigma})^{1/2}$ . As a second parameter we choose the quasiparticle lifetime in the normal state

$$\frac{1}{\tau_s} = c \frac{2\pi N(0)v_s^2}{1 + [\pi N(0)v_s]^2} = 2 \frac{c}{\pi N(0)} \bar{\sigma} .$$

We solve the coupled system consisting of the  $t$ -

matrix equation and the transportlike equations self-consistently, i.e., we replace  $\hat{g}_0$  in Eq. (3.6) by the full quasiclassical  $\hat{g}$  which is to be determined. This Green's function  $\hat{g}$  has the same structure as  $\hat{g}_0$  and the impurity scattering is accounted for in the renormalized arguments,  $\tilde{\omega}$  and  $\tilde{h}$ . In the case of  $s$ -wave scattering we obtain two coupled scalar equations which determine the complex frequency  $\tilde{\omega}$  and magnetic field strength  $\tilde{h}$

$$\begin{aligned} \tilde{\omega} = \omega - \frac{1}{2\tau_s} \frac{\langle g_s \rangle}{\pi} \frac{1 - \bar{\sigma}[1 + (1/\pi^2)\langle g \uparrow \rangle \langle g \downarrow \rangle]}{\{1 - \bar{\sigma}[1 - (1/\pi^2)\langle g \uparrow \rangle^2]\} \{1 - \bar{\sigma}[1 - (1/\pi^2)\langle g \downarrow \rangle^2]\}} , \\ \tilde{h} = h + \frac{1}{2\tau_s} \frac{\langle g_v \rangle}{\pi} \frac{1 - \bar{\sigma}[1 - (1/\pi^2)\langle g \uparrow \rangle \langle g \downarrow \rangle]}{\{1 - \bar{\sigma}[1 - (1/\pi^2)\langle g \uparrow \rangle^2]\} \{1 - \bar{\sigma}[1 - (1/\pi^2)\langle g \downarrow \rangle^2]\}} , \end{aligned} \quad (3.10)$$

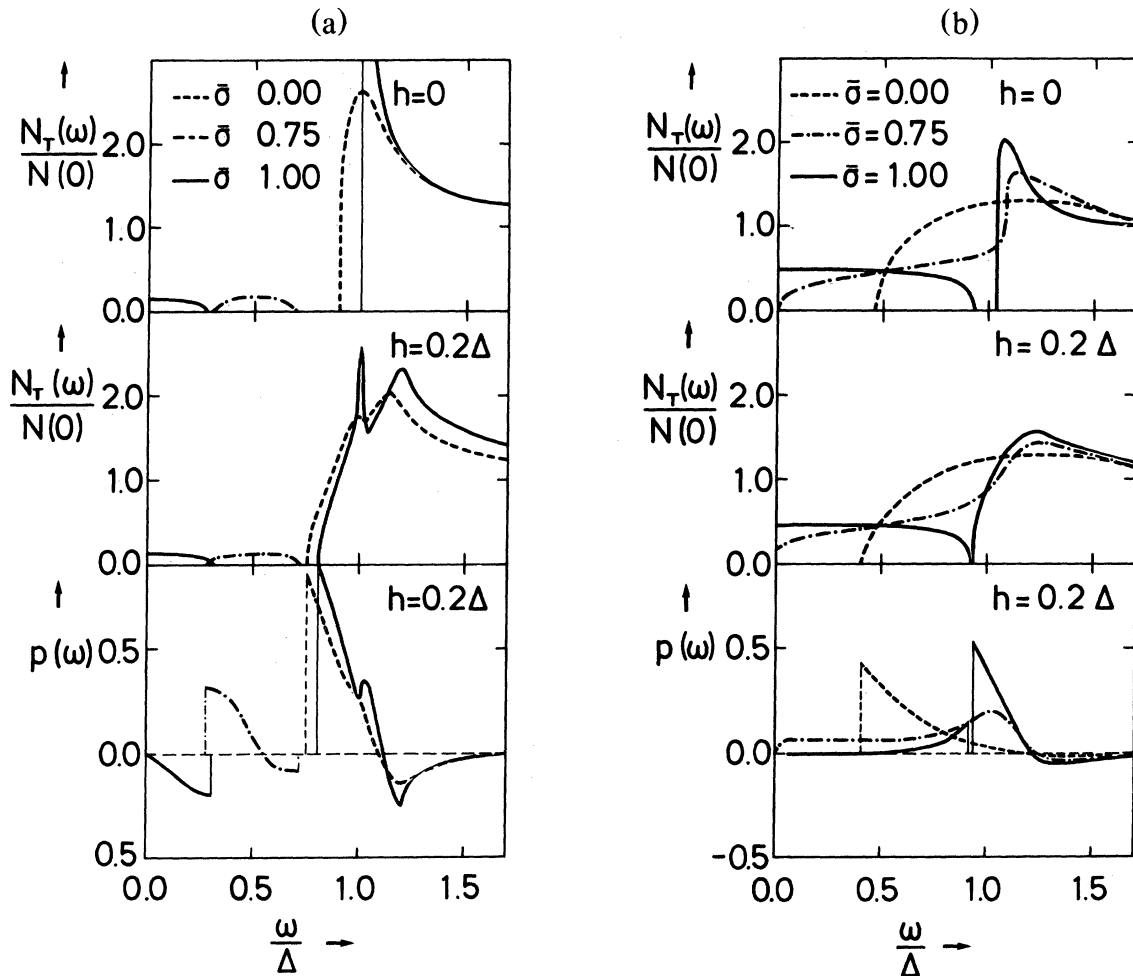


FIG. 3. Total densities of states,  $N_T(\omega)/N(0)$ , and polarization,  $p(\omega)$ , in a bulk triplet superconductor doped with impurities (a)  $1/2\tau_s = 0.01$ , (b)  $1/2\tau_s = 0.20$ .

where we introduced

$$\begin{pmatrix} \langle g \uparrow \rangle \\ \langle g \downarrow \rangle \end{pmatrix} = \langle g_s \rangle \pm \langle g_v \rangle .$$

For a fixed quasiparticle lifetime  $\tau_s$ , the shape of the excitation spectrum may depend quite substantially on the strength of the individual scattering potentials  $\bar{\sigma}$  which determines the position of the impurity band. This parameter dependence may be estimated from Ref. 5 where pair breaking from magnetic impurities in conventional *s*-wave superconductors is discussed.

In the presence of a magnetic field the quasiparticle excitations of the isotropic BW state are not eigenfunctions of a fixed spin projection and consequently potential scattering from the impurities mixes together different spin states. Characteristic features of the excitation spectrum [e.g., the two peaks at  $\omega = |\bar{\Delta}|$  and  $\bar{\omega} = (|\bar{\Delta}| + |\hbar|)$ ] are smeared out by quasiparticle lifetime effects and spin relaxation as can be seen from Fig. 3. For sufficiently high inverse lifetimes  $1/\tau_s$  these two peaks merge together into one broad hump. The critical value depends upon the strength of the individual potentials and on the magnetic field. For  $h = 0.2|\bar{\Delta}|$  the two peak structure is observed up to a value of  $1/2\tau_s < 0.10$  in the unitary limit  $\bar{\sigma} = 1$  whereas it disappears for  $1/2\tau_s > 0.025$  in the weak scattering (Abrikosov-Gorkov) limit. Similar behavior is encountered in singlet superconductors when spin-orbit scattering from nonmagnetic impurities becomes important.<sup>6</sup> There is, however, a crucial distinction between these two cases: Spin-orbit scattering does not suppress *s*-wave superconductivity since it does not violate time reversal invariance whereas momentum scattering in an anisotropic superfluid leads to pair breaking. This is reflected in the formation of the impurity bands the shapes of which are only weakly affected by the magnetic field. (The splitting of the impurity band is observed only in the extremely dilute case, e.g.,  $h = 0.2$ ,  $\bar{\sigma} = 0.75$ ,  $1/2\tau_s = 10^{-3}$ .) From these results we conclude that also in the presence of nonmagnetic impurities a measurement of the bulk density of states would allow us to identify triplet pairing unambiguously.

#### IV. SURFACE RESPONSE

Tunnel junction experiments measure directly the surface density of states at a junction wall. In the expectation that this fact might be exploited, we have focused our surface calculation, to date, on exploring features of this quantity.

For the adoption of a model describing surface effects we once again relied on experience with superfluid <sup>3</sup>He. The gap function is assumed *B* phase in the bulk of the form  $\Delta(\hat{k}) = \Delta \hat{k} \cdot \bar{\sigma} i \sigma_2$  but which

then in the vicinity of the wall generalizes to

$$\Delta_{\parallel}(R) \hat{k}_{\parallel} \cdot \bar{\sigma} i \sigma_2 + \Delta_{\perp}(R) \hat{k}_{\perp} \cdot \bar{\sigma} i \sigma_2 ,$$

where  $\hat{k}_{\parallel}$  refers to components within the surface. The self-energy entering Eq. (2.2) takes the form

$$\hat{\sigma} = \begin{pmatrix} 0 & \Delta \\ \Delta^{\dagger} & 0 \end{pmatrix}$$

and the *p*-wave gap equation may be written

$$\Delta(\hat{k}; \bar{R}) = -gT \sum'_{\epsilon_n} \int \frac{d^2 \hat{k}'}{4\pi} 3 \hat{k} \cdot \hat{k}' f(\hat{k}; R; \epsilon_n) , \quad (4.1)$$

where  $g$  is a coupling constant and  $f$  the anomalous Green's function. Finally, the wall itself was assumed to be a specularly reflecting surface. Whether or not this is the optimal model available is certainly open for discussion, but we may at least reasonably hope that most of the pertinent surface phenomena will appear here as well. The boundary condition in this case takes the simple form

$$\hat{g}(\hat{k}) = \hat{g}(\hat{k}) , \quad (4.2)$$

on the surface, where  $\hat{k} = \hat{k} - 2\hat{n}(\hat{n} \cdot \hat{k})$  ( $\hat{n}$  is the unit normal into the bulk) is the mirror reflected  $\hat{k}$  vector.

The first step in the numerical computation is an explicit specification of the spatially dependent gap function. We chose to solve Eqs. (2.2), (4.1), and (4.2) self-consistently yielding  $\Delta(\bar{R})$  for a specular wall. Concurrently, we employed simple test models for  $\Delta(\bar{R})$  to probe the sensitivity of the system against perturbations. No in depth study of temperature dependence was attempted for this paper, rather we chose two values of  $T$ ,  $T_1 = 0.647 T_c$ , and  $T_2 = 0.838 T_c$  for which the self-consistent gap evaluation was conducted. The structure of the ensuing results is displayed in Fig. 4. To facilitate comparison, the units of energy and length were chosen to be the temperature-independent quantities  $\Delta_0 = \Delta_{\text{bulk}}(T=0)$ , and  $\xi_0 = \hbar v_F / \pi \Delta_0$ . In general, the perpendicular component of the order parameter is suppressed to zero and the parallel components are slightly enhanced as they approach the wall. Roughly speaking, this depression of the perpendicular component acts as a potential well for quasiparticle excitations, and is responsible for the unique and distinguishing character of the density of states. In contrast, *s*-wave pairing is not disrupted by a (nonmagnetic) surface; i.e., a wall does not act as a pair breaking scatterer. Consequently, the order parameter will not be diminished which is the crucial distinction.

For purposes of comparison we present alongside the self-consistently determined data the test case where  $\Delta_{\parallel}$  is held constant at the bulk value and  $\Delta_{\perp}$  proceeds linearly from zero to the bulk value over a

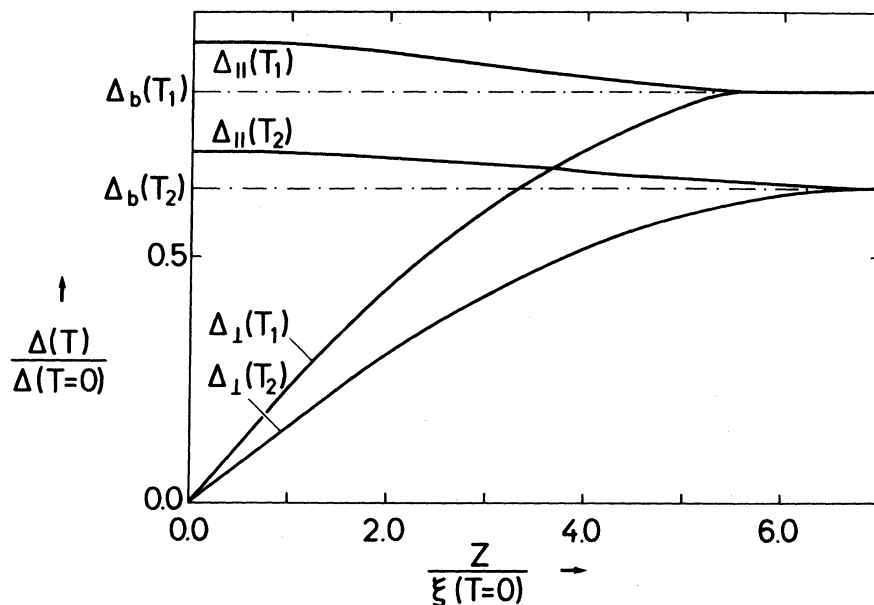


FIG. 4. Parallel and perpendicular components of the order-parameter vector near a specularly reflecting surface for  $T_1 = 0.647T_c$  and  $T_2 = 0.838T_c$ .

distance  $4\xi(T)$ .

Temperature dependence enters the real frequency results only through  $\Delta(T)$ , which acts as a scaling factor for energy and length. Consequently, the model's results offer a comparison of density of states behavior at each temperature merely by rescaling the energy variable. The use of these models was intended principally at observing the sensitivity of the

results to the precise shape of the order parameter, and their display will be labeled "model."

For a given  $\hat{k}$  vector the density of states  $n(\hat{k}, \omega)$  [measured in units of  $N(0)$ ] may contain considerable structure. Dependence on the direction of incidence enters through the angle to the normal  $\cos\theta = \hat{k} \cdot \hat{n}$ . Results for various angles at temperature  $T_1$  reveal typically observed characteristics, and

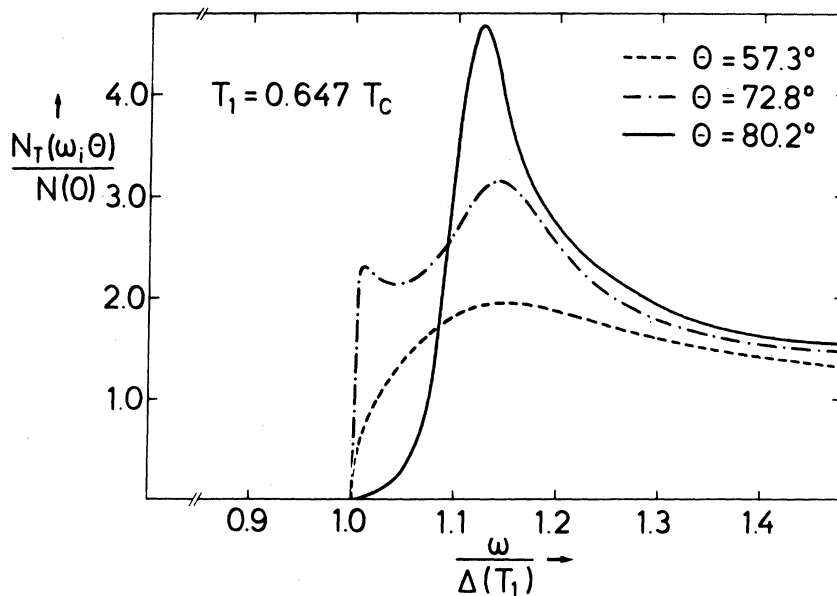


FIG. 5. Comparison of the densities of states,  $N_T(\omega; \theta)/N(0)$ , near a specularly reflecting surface for  $T_1 = 0.647T_c$  and for various angles of incidence.

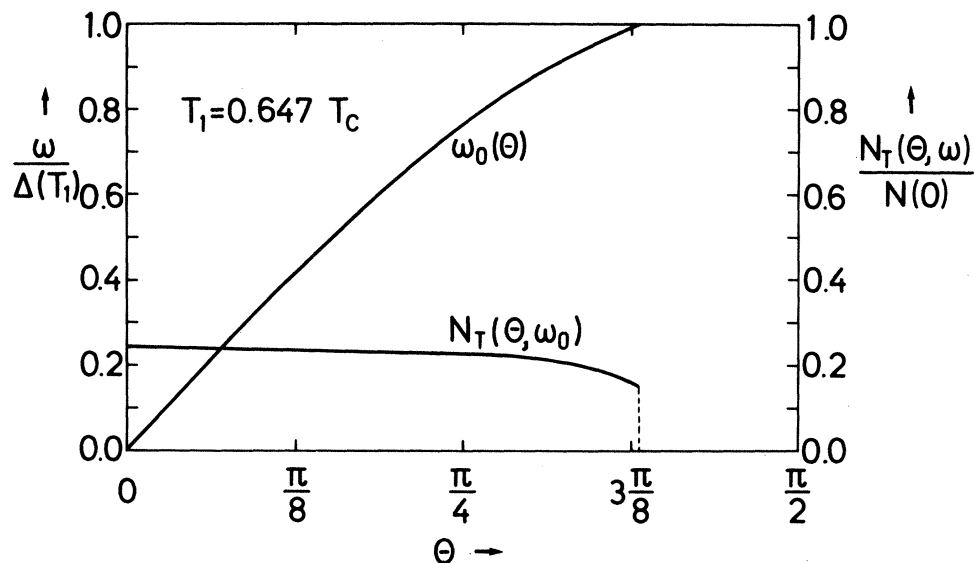


FIG. 6. Dependence on angle of incidence of the position of the bound state,  $\omega_0(\theta)$ , and its weight,  $N_T(\omega_0; \theta)/N(0)$ , for  $T_1 = 0.647 T_C$ .

are displayed in Fig. 5. Incidence at angles between zero (normal) and  $\approx 1.3$  rad yields two particularly conspicuous features. First is the presence of a single bound-state  $\delta$  function peak of significant weight at energies  $\omega_B$  less than  $\Delta_{\text{bulk}}(T)$ . And second, the gentle curve for  $\omega > \Delta$  betrays no square-root singularity that would be typical of the *s*-wave case. This curve overshoots the bulk value in its climb and then relaxes to it over an energy width of a few  $\Delta$ .

The energy of the bound state increases with angle until at a value  $\theta \approx 1.3$  rad the spike merges with the curve above and fades away. For angles nearing this merging value (ever more grazing) one observes, as well, that the "overshoot" mentioned above is developing into a real peak at an energy above  $\approx 1.1\Delta$ . This peak would be the analog of that observed in *s*-wave pairing though no singular behavior is observed here. Figure 6 details the position of the bound-state peak and its weight. The

strong angular dependence manifested here is a direct consequence of the anisotropic nature of the gap on the surface. At non-normal incidence the perpendicular component of  $\Delta$  is "perceived" more strongly than the parallel ones. Since  $\Delta_{\perp}$  has been greatly diminished excitations are possible at energies below  $\Delta$ . With increasing angle the parallel components play an ever more important role. Near parallel incidence they are dominant, as evidenced by the appearance of an *s*-wave-like peak and its position above  $\Delta_{\text{bulk}}$  (in response to the enhancement of  $\Delta_{\parallel}$  on the wall). The model calculations substantiate this picture in detail.

An actual experiment would presumably measure  $n(k, \omega)$  folded against some other quantity. Were the experiment especially sensitive to particles colliding at near-normal incidence, where the discrepancy with *s*-wave pairing is particularly apparent, one might hope that *p*-wave pairing could be clearly marked.

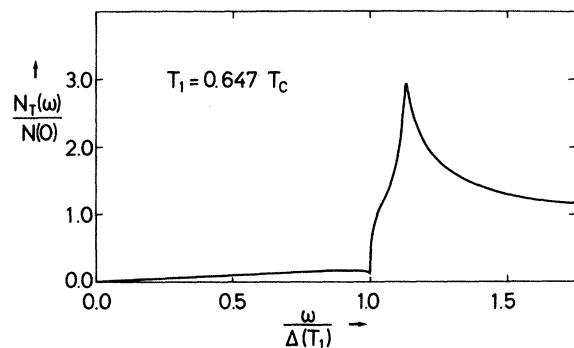


FIG. 7. Integrated density of states near the specularly reflecting wall for  $T_1 = 0.647 T_C$ .

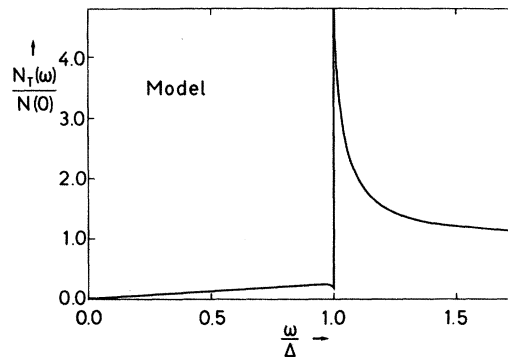


FIG. 8. Density of states obtained from the model order parameter.

We present as well (see Fig. 7) the total density of states integrated over angle. The "model" results (Fig. 8) are quite markedly different and indicate the importance of the most accurate input data possible. An improved calculation would include the effects arising from a diffuse wall. Diffuseness would presumably lead to a suppression of both components at the surface. Test calculations then indicate, in fact, an intensification of the two principal distinguishing features. First, were  $\Delta_{\parallel}$  suppressed we would expect the peak in the integrated density of states above  $\omega = \Delta$  to vanish and, second, we would expect yet more bound states to appear at energies  $\omega < \Delta$ .

In summary, we may reaffirm the speculation of Merservey mentioned at the beginning that surface response ought to serve as a useful tool in the search for *p*-wave superconductors.

## V. CONCLUSIONS

The central result of this paper is the confirmation of Mersevey's idea that a hypothetical triplet superconductor might be identified by means of a tunnel-junction experiment. A magnetic field causes distinctive structures in the excitation spectrum of the ideally clean bulk system. Pair-breaking effects at non-magnetic impurities will tend to wash out these features. This effect is, however, accompanied by the formation of impurity states which allows us to distinguish a triplet-paired system from a singlet superconductor with strong spin-orbit scattering. The bulk effects cannot be measured directly in a tunneling experiment. The reason is that the anisotropic  $l \neq 0$  state is, unlike an  $l = 0$  state, radically altered by surface effects at the tunnel junction. Our fully self-consistent calculation for the order parameter near a surface showed that the perpendicular component is suppressed at the specular wall, as was to be expected from its behavior in the Landau-Ginsburg regime.<sup>7</sup> Consequently, bound states appear filling up the excitation gap, and the square-root singularity vanishes. Thus the total density of states curve at the wall definitely differs from the well-known *s*-wave shape, even in the field-free case where the bulk densities of states do not differ at all. However, a remarkably sharp maximum remains and

accounting for finite energy resolution one might object that this structure is not likely to be distinguished experimentally from an *s*-wave singularity. In this case, a clear distinction between *s*- and *p*-wave pairing is possible through the magnetic effects discussed in Sec. III. The situation changes when a finite surface roughness, probably unavoidable in tunnel junctions, is taken into account.

The appearance of pronounced bulklike structures in the surface density of states is an artifact of the specular wall model, and this prominent feature ought to disappear near a rough surface. Unfortunately, detailed numerical investigations are still lacking, mainly because of the highly complex surface problem, but the qualitative behavior can be inferred from the following considerations: A careful analysis of the angular dependence evidenced that the main contributions to the prominent peak come from quasiparticle excitations at almost grazing incidence for which the parallel components of the order parameter dominate. For specular reflection, these components do not vanish at the wall but are even slightly enhanced. A diffusely reflecting wall tends to suppress *all* components of the order parameter. Consequently quasiparticles at all angles will experience the effects of a surface-suppressed order parameter and the corresponding total density of states curve should parallel the one encountered at normal incidence at a specular wall where no pronounced structure above  $\Delta$  survives. This yields a very definite and easy to measure difference between *s*-wave and higher *l* pairing. With a rough tunnel junction, and we expect all conventional junctions to be rough, it will be impossible to see a well-defined gap for an  $l \neq 0$  superconductor. The density of states is too much deformed by surface pair-breaking effects to resemble anything like a BCS-type structure, an effect which is absent for *s*-wave superconductors. The exact details, however, require further investigations including a quantitative study of surface roughness and its influence on superfluid properties near a wall.

## ACKNOWLEDGMENTS

We would like to thank Professor Dierk Rainer for many helpful discussions along the whole course of this work.

\*Present address: Los Alamos Scientific Laboratory, P.O. Box 1663, Los Alamos, N.M. 87545.

<sup>1</sup>R. Merservey (private communication).

<sup>2</sup>L. J. Buchholtz and D. Rainer, Z. Phys. B **35**, 151 (1979).

<sup>3</sup>J. W. Serene and D. Rainer, Phys. Rev. B **17**, 2901 (1978).

<sup>4</sup>H. Shiba, Prog. Theor. Phys. **40**, 435 (1968).

<sup>5</sup>J. Zittartz, A. Bringer, and E. Müller-Hartmann, Solid State Commun. **10**, 513 (1972).

<sup>6</sup>P. Fulde, Adv. Phys. **22**, 667 (1973).

<sup>7</sup>V. Ambegaokar, P. G. de Gennes, and D. Rainer, Phys. Rev. A **9**, 2676 (1974).